universe

IMPACT FACTOR 2.6

CITESCORE 5.2

Article

# Differing Manifestations of Spatial Curvature in Cosmological FRW Models

Meir Shimon and Yoel Rephaeli

MDPI

https://doi.org/10.3390/universe11050143

universe

MDPI

*Article*

# Differing Manifestations of Spatial Curvature in Cosmological FRW Models

**Meir Shimon [1,*] and Yoel Rephaeli [1,2]**

[1] School of Physics and Astronomy, Tel Aviv University, Tel Aviv 69978, Israel; yoelr@tauex.tau.ac.il
[2] Department of Physics, University of California, La Jolla, San Diego, CA 92093, USA
* Correspondence: meirs@tauex.tau.ac.il

**Abstract:** We found statistical evidence for a mismatch between the (global) spatial curvature parameter $K$ in the geodesic equation for incoming photons and the corresponding parameter in the Friedmann equation that determines the time evolution of the background spacetime and its perturbations. The mismatch, hereafter referred to as 'curvature slip', was especially evident when the SH0ES prior of the current expansion rate was assumed. This result is based on joint analyses of cosmic microwave background (CMB) observations with the PLANCK satellite (P18), the first year results of the Dark Energy Survey (DES), baryonic oscillation (BAO) data, and at a lower level of significance, the Pantheon SNIa (SN) catalog as well. For example, the betting odds against the null hypothesis were greater than $10^7$:1, 1400:1 and 1000:1 when P18+SH0ES, P18+DES+SH0ES and P18+BAO+SH0ES were considered, respectively. Datasets involving SNIa weakened this curvature slip considerably. Notably, even when the SH0ES prior was not imposed, the betting odds for the rejection of the null hypothesis were 70:1 and 160:1 in cases where P18+DES and P18+BAO were considered. When the SH0ES prior was imposed, the global fit of the modified model (that allows for a nonvanishing 'curvature slip') strongly outperformed that of ΛCDM, being manifested by significant deviance information criterion (DIC) gains ranging between 7 and 23, depending on the dataset combination considered. Even in comparison with KΛCDM, the proposed model resulted in significant, albeit smaller, DIC gains when SN data were excluded. Our finding could possibly be interpreted as an inherent inconsistency between the (idealized) maximally symmetric nature of the FRW metric and the dynamical evolution of the GR-based homogeneous and isotropic ΛCDM models. As such, this implies that there is apparent tension between the metric curvature and the curvature-like term in the time evolution of the redshift.

**Keywords:** cosmology; spatial curvature; curvature slip; anomaly



Academic Editor: Antonino Del Popolo

Received: 27 March 2025
Revised: 23 April 2025
Accepted: 27 April 2025
Published: 30 April 2025

**Citation:** Shimon, M.; Rephaeli, Y. Differing Manifestations of Spatial Curvature in Cosmological FRW Models. *Universe* **2025**, *11*, 143. https://doi.org/10.3390/universe11050143



## 1. Introduction

On the largest observable scales, the Universe appears to be extremely isotropic around us. Augmented by the Cosmological Principle, this ('local') isotropy is endowed to every observer at rest in the cosmic microwave background (CMB) frame. The corresponding spacetime is uniquely described by the Friedmann–Robertson–Walker (FRW) metric. Space in the latter has either closed, flat or open geometry. If, in addition, it is assumed that gravitation is governed by general relativity (GR), then this background spacetime is shaped by its homogeneous and isotropic matter content. Incoming photons propagating in curved space trace its global geometry, and observational determination of various (angular diameter, luminosity distance, etc.) distance-redshift relations enable inference of

the matter content of the Universe. The CMB anisotropy and polarization depend on both the matter content and geometry.

The currently favored cosmological model, ΛCDM, is spatially flat, and its energy content consists of ∼69% dark energy (DE), 31% non-relativistic (NR) matter—[5% baryons and 26% cold dark matter (CDM)]—as well as a residual amount $\lesssim 0.1\%$ CMB radiation and relativistic (and possibly also NR) neutrinos. The consensus 'vanilla' ΛCDM model, characterized by only six parameters, emerged from joint analyses of various cosmological datasets that include mainly CMB anisotropy and polarization, galaxy clustering and galaxy shear maps, type Ia supernovae luminosity distance measurements and baryonic oscillations (BAOs). However, these models are not fully consistent with each other. Perhaps the most glaring example is the disparity between the Planck satellite CMB data, which favor a spatially closed cosmological model at $\sim 3\sigma$ statistical significance on the one hand, and BAO data, which strongly favor flat space on the other hand (e.g., [1–4]). Their combination considerably weakens the case for a closed Universe (e.g., [5]), resulting in the best fit 'model of choice': the flat ΛCDM model.

A spatially non-flat Universe would seem to be unnatural [6] (i.e., fine-tuned) in either case of a curvature radius much larger or much smaller than the present horizon size of the observable Universe. For example, if the initial conditions of the Universe are set to the Grand Unified Theories (GUT) scale, then the curvature radius must have been fine-tuned at a precision level of one part in a trillion so as to be either a quadrillion times larger or smaller than the horizon size of the observable Universe at the present time. This is the consensus understanding of the 'flatness problem' [6], although there are counterarguments that lend some support to the claim that this is not really problematic for the original Hot Big Bang model [7–12]. This, as well as the 'horizon problem', have provided the main motivation for the inflationary scenario. Observationally, whether space is flat or closed is still an unsettled issue (e.g., [1,13–33]), but the far-reaching implications of a closed Universe cannot be overstated (e.g., [3]).

From the cosmic inflation perspective (e.g., [34]), a spatially flat Universe is strongly favored (although open- (e.g., [35–38]) and closed-inflation (e.g., [39]) models were proposed). If so, then the PLANCK dataset stands out and is especially at odds with the BAO dataset in favoring a non-flat Universe. The challenge is that only a probe of an extremely large scales can result in a credible inference of (or bounds on) the curvature radius. Perhaps the most precise and well-understood cosmological probe is measurements of CMB anisotropy and polarization, and thus only satellite-based measurements are capable of meaningfully constraining the curvature radius. At present, the Planck database is most optimally suited for this. While joint analyses of the current CMB+BAO datasets tilt the balance toward a spatially flat space, it is arguably problematic to put too much weight on this conclusion, mainly because the current CMB+BAO datasets are internally inconsistent (e.g., [1]). Clearly, global geometry is a critical property of the Universe; whereas values of the other basic parameters of the cosmological standard model (SM) affect the (temporal) evolution of physical processes, only the curvature and DE parameters determine its global geometry and future evolution.

In this paper, we explore certain hitherto unexplored extensions to the time redshift $t(z)$, the relation of the standard FRW-based treatment, and the $r(t)$ relation that, in general, departs from the geodesic equation. Basically, we allow for $t(z)$ to differ from the relation obtained from the Friedmann equation (i.e., it does not depend solely on the matter content of the Universe). In other words, we employ $t(z)$ relations in our analysis that, under the assumption of isotropy and homogeneity, represent a clear violation of local energy-momentum conservation (i.e., we basically abandon the GR-based framework). Energy-momentum non-conservation is a generic feature of various theories of gravitation [40],

the most common (and well known) of which are scalar-tensor theories. Other examples are Rastall gravity [41], unimodular gravity [42,43], and other theories [44–47]. Another possibility is that the degree of large-scale isotropy of the Universe is inconsistent [48] with the underlying assumption characterizing the FRW spacetime. Perhaps unexpectedly, our analysis results point toward phenomenological parameters in the $r(z)$ relation that depart by up to $\sim 4\sigma$ from their canonical values, depending on the dataset combination used and the assumed priors. This result adds to other anomalies or tensions that have been long recognized to afflict the cosmological SM (e.g., the 'lensing anomaly'), the $\sigma_8/S_8$ tension of the CMB with large scale clustering probes, and the 'Hubble tension' (e.g., [2,31]).

We employ the deviance information criterion (DIC) in assessing the relative likelihood of each proposed model in comparison with both the standard flat ΛCDM and its 'curved' extension KΛCDM models. We find that depending on the specific dataset combinations, the proposed models can be mildly or even strongly favored over ΛCDM, thereby substantiating our finding that the $t(z)$ relation does not depend solely on the matter content from a global parameter analysis perspective.

This paper is organized as follows. In Section 2, we summarize a few basic results of the SM for reference in future sections and for setting the notation. In Section 3, we describe our proposed modifications, model comparison analysis and results. Our conclusions are discussed in Section 4, and our work is summarized in Section 5. Throughout, we adopt units such that the speed of light, where $c \equiv 1$.

## 2. The Benchmark Standard Model

On the largest observable scales, the Universe has been found to be highly isotropic to within one part in $10^5$. The implication of this observation is greatly widened by adoption of the Cosmological Principle, essentially stating that the Universe appears isotropic (and therefore uniform) to every 'fundamental' observer. The FRW metric of such a (maximally symmetric) space is expressed in terms of the line element

$$ds^2 = -dt^2 + a^2\Big[\frac{dr^2}{1-Kr^2} + r^2(d\theta^2 + \sin^2\theta d\varphi^2)\Big], \tag{1}$$

where $a = a(t)$ is the scale factor, $K$ is the spatial curvature parameter, and (with no loss of generality) the origin of spatial coordinates is set to be at the observer. Incoming radial null geodesics in this spacetime integrate to

$$r(\eta) = \begin{cases} \frac{\sin[\sqrt{K}(\eta_0-\eta)]}{\sqrt{K}} & ;K>0 \\ \eta_0 - \eta & ;K=0 \\ \frac{\sinh[\sqrt{-K}(\eta_0-\eta)]}{\sqrt{-K}} & ;K<0, \end{cases} \tag{2}$$

where $\eta \equiv \int \frac{dt}{a(t)}$ is the conformal time and $\eta_0$ is its present value.

In the GR-based SM, use of the FRW metric in the field equations for the adiabatically evolving Universe can be summarized in a single Friedmann equation:

$$H^2 + \frac{K}{a^2} = \frac{8\pi G\rho(a)}{3}, \tag{3}$$

where $H \equiv \dot{a}/a$, $\dot{a} \equiv \frac{da}{dt}$, $G$ is the Universal gravitational constant, and $\rho$ is the total energy density. Assuming that the various contributions to the cosmic energy budget do not mutually interact, then the continuity equation applied to the ith species is

$$\dot{\rho}_i + 3(1+w_i)H\rho_i = 0, \tag{4}$$

where $w_i$ is the equation of state (EOS) parameter of the ith species, which integrates into

$$\rho_i(a) = \rho_{i,0} \exp\Big[-\int 3(1+w_i(a))\frac{da}{a}\Big]. \tag{5}$$

In addition, if it is assumed that $w_i(a) = w_i$ is fixed (an assumption that breaks down in the case of neutrinos when they turn NR once the Universe cools down below a temperature equivalent to their rest masses), an assumption that is *not* made in actual computations, then $\rho_i a = \rho_{i,0} a^{-3(1+w_i)}$, and the total energy density is

$$\rho(a) = \sum_i \rho_{i,0} a^{-3(1+w_i)}. \tag{6}$$

Substituting Equation (6) into Equation (3) and integration yield the basic expression for $t(a)$ or, equivalently, $\eta(z)$, where $a \equiv (1+z)^{-1}$. Use of the latter expressions in Equation (2) results in the following $r(z)$ relation:

$$H_0 r(z) = \begin{cases} \frac{\sin(\sqrt{-\Omega_k}\mathcal{D})}{\sqrt{-\Omega_k}} & ;\Omega_k < 0, K > 0 \\ \mathcal{D} & ;\Omega_k = 0, K = 0 \\ \frac{\sinh(\sqrt{\Omega_k}\mathcal{D})}{\sqrt{\Omega_k}} & ;\Omega_k > 0, K < 0, \end{cases} \tag{7}$$

where $\Omega_k \equiv -K/H_0^2$ and

$$\begin{aligned} \mathcal{D}(z;\{\Omega_{i,0}\}) &\equiv H_0(\eta_0 - \eta) = \int_0^z \frac{dz'}{E(z')}, \\ E^2(z') &\equiv \sum_i \Omega_{i,0}(1+z')^{3(1+w_i)}. \end{aligned} \tag{8}$$

Here, $\{\Omega_{i,0}\}$ collectively denotes the various $\Omega_{i,0}$, which are the respective values of the energy densities at present, expressed in critical density units, and $\rho_c \equiv 3H_0^2/(8\pi G)$, including $\Omega_k$ with an effective EOS $w_{k,eff} = -1/3$. Specifically, in a Universe containing only photons, dust, DE, and curvature, we have

$$E(z) \equiv \sqrt{\Omega_r(1+z)^4 + \Omega_m(1+z)^3 + \Omega_k(1+z)^2 + \Omega_\Lambda}. \tag{9}$$

It should be noted that $\Omega_k$ controls both the *dynamics* of cosmic evolution (via the Friedmann equation, shown in Equation (3), or equivalently Equation (9)) and the *kinematics* (or perhaps more precisely referred to as the 'optics') of incoming photons (via the geodesic equation, shown in Equation (2)). It is also important to keep in mind that whereas the optics only depends on the form of the metric, essentially reflecting the spatial symmetry, the dynamics depends on the underlying theory of gravitation (which relates the geometry to the underlying energy-momentum content) as well.

## 3. Modified Curvature SM

In the present work, we explore the implications of phenomenologically modifying the time-redshift $t(z)$ and distance-time $r(t)$ relations on cosmological scales (on which the assumption of homogeneity and isotropy is still assumed). The SM $t(z)$ relation follows from the Friedmann equation (i.e., local energy-momentum conservation). In addition, the $r(t)$ relation describes the trajectories of incoming radiation along null geodesics. The latter describes the kinematics of test particles under the premise of energy-momentum conservation. Combining $r(t)$ and $t(z)$ yields the observable $r(z)$ relation.

Here, we replace Equation (7) with

$$H_0 r(z) = \begin{cases} \frac{\sin(\sqrt{-\omega_k}\mathcal{D})}{\sqrt{-\omega_k}} & ;\omega_k < 0 \\ \mathcal{D} & ;\omega_k = 0 \\ \frac{\sinh(\sqrt{\omega_k}\mathcal{D})}{\sqrt{\omega_k}} & ;\omega_k > 0 \end{cases} \tag{10}$$

where we introduce a new parameter $\omega_k$ while leaving $\mathcal{D}$ (Equation (8)) unchanged. In general, we do *not* require $\omega_k$ to be equal to $\Omega_k$ in Equations (9) and (10) and define $\kappa \equiv \omega_k - \Omega_k$ as a derived parameter in our modified models. Clearly, nested within these models are K$\Lambda$CDM, if indeed $\omega_k = \Omega_k$, and flat $\Lambda$CDM in the particular case where $\omega_k = \Omega_k = 0$. In a similar vein to the addition of the cosmological constant to the SM as discussed above, we introduce the free dimensionless parameter $\kappa$ coupled to a specific redshift dependence (as shown in Equations (9) and (10)) but with neither energetic interpretation nor any perturbation imprints (i.e., it does not cluster), much like DE (assuming it is a cosmological constant). Obviously, the likelihood of $\kappa \neq 0$ will be determined by contrasting the modified model with the various datasets.

Whereas, by their very nature, cosmological observables typically probe Equation (10), the Sandage–Loeb effect (also known as the *redshift drift effect* [49–51]) is sensitive to $\frac{dz}{dt}$ and is therefore directly dependent on the Friedmann equation (Equation (9)). While Equation (10) depends on both $\Omega_k$ and $\omega_k$ (as well as $\Omega_m$), Equation (9) depends solely on $\Omega_k$. Future measurements of the redshift drift, when combined with precision measurements of $r(z)$, could in principle allow for a clean separation of $\Omega_k$ and $\omega_k$. However, undertaking such an endeavor would be challenging, given that the redshift drift signal is extremely weak over typical observational timescales.

Because no perturbations are considered in the value of $\Omega_k$, in our analysis, $\kappa$ is a truly anomalous parameter essentially devoid of physical meaning. In this specific sense, it plays a role similar to other phenomenological parameters that have been considered in various generalizations of the SM, such as the lensing anomaly parameter $A_L$ (e.g., [52]), the dipole and integrated Sachs–Wolfe (ISW) anomaly parameters (e.g., [53,54]), and the CMB temperature mismatch parameter when local priors on $H_0$ are assumed [55–57]. The parameter $\kappa$ should be consistent with zero if GR and the underlying assumption of the Cosmological Principle are not just qualitatively but also quantitatively valid. In principle, since $\Omega_k$ appears in Equation (9) as a contribution of an effective fluid with equations of state, where $w = -1/3$, it could be viewed as the combined effect of curvature and a 'K-matter contribution' (save for the fact that it is unperturbed in our analysis) (e.g., [58]). However, as we will see below, it turns out that our analysis of the (present) observational datasets yields $\kappa > 0$, further reducing the likelihood for it to be a new exotic matter contribution candidate. In general terms, the 'null hypothesis' is rejected to the extent that $\kappa$ statistically departs from zero.

One possible explanation for the nonvanishing phenomenological parameter $\kappa$ could be that the FRW spacetime metric is an over-idealization of spacetime that fails on sufficiently small scales. This could possibly indicate that when averaging over sufficiently small scales, second-order perturbations do not vanish and can back-react on a smoothed out background. In particular, it can manifest in the form of effective spatial curvature or K-matter, DE, and also stress-like contributions in the volume-averaged Friedmann equation. This does not readily and unequivocally reflect on the effective spacetime metric. These effects could not only tilt the balance between the various terms in the volume-averaged Friedmann equation but also affect the growth of the structure, thereby biasing the inferred cosmological parameters, with the curvature parameter included (e.g., [59–76]).

### 3.1. Models and Datasets

We carried out an extensive statistical analysis in order to determine the most probable ranges of the extended parameter set of the proposed modifications to the SM. To the 'vanilla' *fundamental* model parameters $\boldsymbol{\theta_{MC}}$, $\Omega_b h^2$, $\Omega_c h^2$, $\tau$, $A_s$, and $n_s$, we add both $\Omega_k$ and $\omega_k$. The parameter $\kappa$ is a derived parameter. Additional relevant derived parameters that will be of interest to us here are $H_0$, $S_8$, and $\sigma_8$, especially in light of the well-known tensions involving these parameters when inferred from various dataset combinations. The models considered in this work are summarized in Table 1.

**Table 1.** Models explored in this work.

| | |
|---|---|
| `Model 1` ($\Lambda$CDM) | $\Omega_k = 0 = \omega_k$ |
| `Model 2` (K$\Lambda$CDM) | $\Omega_k \equiv \omega_k$ |
| `Model 3` | $\Omega_k \neq 0, \omega_k \neq 0$ |
| `Model 4` | $\Omega_k \neq 0$ |
| `Model 5` | $\omega_k \neq 0$ |

The datasets employed in this analysis constitute the standard commonly adopted set (in model testing), which is included (along with the corresponding likelihood functions) as part of the CosmoMC 2021 package. These include the CMB Planck 2018 data [77], DES 1 yr [78], BAO (data compilation from BOSS DR12 [79], MGS [80], and 6DF [81]), and Pantheon data (catalog of 1048 SNIa in the redshift range of $z \lesssim 2$ [82]). The entire Planck dataset was included, with a multipole range of $2 < l < 2500$ covered by the `plikHM_TTTEEE`, `lowl`, and `lowE` likelihood functions.

As in our previous (somewhat) related work [57], we considered the P18, P18+DES, P18+BAO, P18+SN, and P18+BAO+SN dataset combinations, each of which we performed the analysis with and without the SH0ES prior on $H_0$ for. Sampling from posterior distributions was performed using the fast-slow dragging algorithm with a Gelman–Rubin convergence criterion $R - 1 < 0.02$ (where R is the scale reduction factor). Testing the curved space model (with the new parameters included) using only the Planck dataset (without the SH0ES prior) did not satisfy this convergence criterion. Therefore, the results for this case were not considered in this work.

### 3.2. Results

For each of the five models described above, we computed the DIC for each dataset combination. The DIC is defined as [83]

$$DIC \equiv 2\bar{\chi^2}(\theta) - \chi^2(\bar{\theta}), \tag{11}$$

where $\theta$ is the vector of free model parameters and bars denote averages over the posterior distribution $P(\theta)$. According to the 'Jeffreys scale' convention, a model characterized by $\Delta$DIC that is lower with respect to a reference model by $<$1, 1.0–2.5, 2.5–5.0, and $>$5 would be considered inconclusively, weakly-to-moderately, moderately-to-strongly, or decisively favored [83] over the reference model, respectively.

Our quantitative DIC results are summarized in Tables 2 and 3. Specifically, when considering dataset combinations with the SH0ES prior, the fits for `Model 3` yielded DIC values lower by 7–23 in comparison with those for `Model 1`. When the SH0ES prior was excluded, `Model 3` was significantly favored for the dataset combinations P18+DES and P18+SN, with DIC gains of eight and seven, respectively, but did not outperform the `Model 1` fits with the dataset combinations P18+BAO, and P18+SN+BAO. Even when

compared with `Model 2`, the `Model 3` fits were better when the SH0ES prior was included. When the SH0ES prior was excluded, `Model 1` and `Model 2` yielded quite similar DIC values (except in the case of P18 data alone, when `Model 2` was strongly favored over `Model 1`, as is shown in Table 2). Therefore, `Model 3` improved over `Model 2` to about the same extent that it improved over `Model 1`. `Model 3` was found to be favored over `Model 4` and `Model 5` for its fits for all dataset combinations with the SH0ES prior.

**Table 2.** DIC values for the various models and dataset combinations. The references, Model 1 and Model 2, are the flat ΛCDM and KΛCDM models, respectively.

| Datasets | `Model 1` | `Model 2` | `Model 3` | `Model 4` | `Model 5` |
|---|---|---|---|---|---|
| P18 | 2799.4 | 2791.0 | – | 2800.1 | 2791.3 |
| | | −8.3 | – | 0.7 | −8.1 |
| P18+DES | 3339.8 | 3338.4 | 3331.6 | 3338.4 | 3339.2 |
| | | −1.3 | −8.1 | −1.3 | −0.6 |
| P18+BAO | 2805.9 | 2806.5 | 2805.9 | 2806.8 | 2806.4 |
| | | 0.6 | 0 | 0.9 | 0.5 |
| P18+SN | 3834.8 | 3835.0 | 3827.7 | 3835.9 | 3835.7 |
| | | 0.2 | −7.0 | 1.1 | 0.9 |
| P18+SN+BAO | 3840.8 | 3841.3 | 3841.7 | 3841.3 | 3841.4 |
| | | 0.5 | 0.9 | 0.5 | 0.6 |

**Table 3.** Same as Table 2, but with the SH0ES prior included.

| Datasets | `Model 1` | `Model 2` | `Model 3` | `Model 4` | `Model 5` |
|---|---|---|---|---|---|
| P18+SH0ES | 2819.3 | 2809.3 | 2795.7 | 2804.8 | 2807.8 |
| | | −10.0 | −23.6 | −14.5 | −11.6 |
| P18+DES+SH0ES | 3354.6 | 3342.0 | 3331.9 | 3338.4 | 3340.1 |
| | | −12.6 | −22.7 | −16.2 | −14.5 |
| P18+BAO+SH0ES | 2824.8 | 2821.5 | 2812.2 | 2818.4 | 2820.9 |
| | | −3.3 | −12.6 | −6.4 | −3.9 |
| P18+SN+SH0ES | 3853.8 | 3844.9 | 3843.1 | 3845.0 | 3844.2 |
| | | −8.9 | −10.7 | −8.8 | −9.6 |
| P18+SN+BAO+SH0ES | 3859.4 | 3856.8 | 3852.4 | 3854.3 | 3856.0 |
| | | −2.6 | −7.0 | −5.2 | −3.4 |

Whereas the ultimate model comparison test must consider the overall model fitness to data, as quantified by the corresponding DIC values in Tables 2 and 3, it is sometimes useful to compare the results for 'anomaly' parameters, which should be identically zero in the reference model (flat ΛCDM). Significant evidence in the data for the addition of an 'anomaly' parameter is indicative of underperformance of the reference model in comparison with the new modified models. The significance of statistical evidence for such an anomaly parameter is usually reported in terms of percentiles or equivalently in terms of 'betting odds' against a finite value for the parameter. We chose the latter option, and the results are listed in Tables 4 and 5. For example, in Table 5, we report the corresponding results for the two fundamental parameters $\Omega_k$ and $\omega_k$, as well as for the derived parameter $\kappa$. It is clear from the table that $\kappa$ was, in general, a better diagnostic of the departures from the reference model than either $\Omega_k$ or $\omega_k$. It is also evident from Table 5 that whereas KΛCDM outperformed flat ΛCDM in virtually all dataset combinations considered in the

present work when the SH0ES prior was imposed (open geometry), as well as in the case of P18 and P18+DES even with the SH0ES prior excluded (closed geometry), `Model 5` and `Model 4` did so even more significantly. We stress again that focusing on a single parameter might be misleading, given that the ultimate test is the 'volume' of the likelihood function in parameter space, where the smaller the volume, the better the fit to the data. Indeed, this was gauged by the DIC values reported in Tables 2 and 3. The general conclusions and trends deduced from Tables 4 and 5 bode well given the results that are shown in Tables 2 and 3.

**Table 4.** Betting odds against $\Omega_k \neq 0$, $\omega_k \neq 0$, and $\kappa \neq 0$ in Model 3 for various dataset combinations. Whereas either $\Omega_k \neq 0$ or $\omega_k \neq 0$ ruled out flat ΛCDM, $\kappa \neq 0$ ruled out both flat ΛCDM and KΛCDM.

| **Dataset** | $\boldsymbol{\Omega_k}$ | $\boldsymbol{\omega_k}$ | $\boldsymbol{\kappa}$ |
|---|---|---|---|
| P18+SH0ES | 1:500 | 1:20 | 1:10,000,000 |
| P18+DES+SH0ES | 1:300 | 1:5 | 1:1400 |
| P18+BAO+SH0ES | 1:1250 | 1:25 | 1:1000 |
| P18+SN+SH0ES | 1:7 | fair | 1:14 |
| P18+BAO+SN+SH0ES | 1:20 | fair | 1:25 |
| P18 | – | – | – |
| P18+DES | 1:50 | 1:7 | 1:70 |
| P18+BAO | 1:4 | fair | 1:5 |
| P18+SN | 1:200 | 1:200 | 1:160 |
| P18+BAO+SN | fair | fair | fair |

**Table 5.** Betting odds against either $\Omega_k \neq 0$ (Model 4) or $\omega_k \neq 0$ (Model 5) in the data. For reference, betting odds against $\Omega_k \neq 0$ in KΛCDM (Model 2) are shown.

| Dataset | `Model 2` | `Model 4` | `Model 5` |
|---|---|---|---|
| P18+SH0ES | 1:300 | 1:100,000 | 1:100,000 |
| P18+DES+SH0ES | 1:2500 | 1:100,000 | 1:1250 |
| P18+BAO+SH0ES | 1:14 | 1:100 | 1:20 |
| P18+SN+SH0ES | 1:300 | 1:500 | 1:500 |
| P18+BAO+SN+SH0ES | 1:16 | 1:50 | 1:20 |
| P18 | 1:500 | 1:4 | 1:1100 |
| P18+DES | 1:4 | 1:12 | 1:5 |
| P18+BAO | fair | fair | fair |
| P18+SN | fair | fair | fair |
| P18+BAO+SN | fair | fair | fair |

Triangle plots for the selected cosmological parameters inferred from fitting `Model 3` to various dataset combinations are shown in Figure 1. There is a clear correlation between $\kappa$ and $\Omega_b h^2$, $\Omega_\Lambda$, and $\sigma_8$ and anticorrelation with $\Omega_c h^2$, $\Omega_k$, and $\omega_k$. For $H_0$, $\Omega_m$, and $S_8$, both correlations and anticorrelations can be seen, depending on the data combination used. If $S_8$ rather than $\sigma_8$ better captured the impact of growth of the structure on the cosmological observables considered in this work, especially the DES dataset, then it is evident from Figure 1 that once $\kappa$ was allowed to freely vary, the data favored lower $S_8$ and higher $H_0$ values, which were even well beyond those obtained with KΛCDM and surely those obtained

with flat ΛCDM. Specifically, these parameters inferred from fitting `Model 3` to P18+DES resulted in $S_8 = 0.773 \pm 0.017$ and $H_0 = 76.5 \pm 3.0$ km/sec/Mpc at a 68% confidence level. For reference, when the same dataset was fitted with KΛCDM (flat ΛCDM), we obtained $S_8 = 0.795 \pm 0.016$ ($0.8018 \pm 0.0066$) and $H_0 = 70.1 \pm 1.7$ ($68.16 \pm 0.48$) km/s/Mpc.

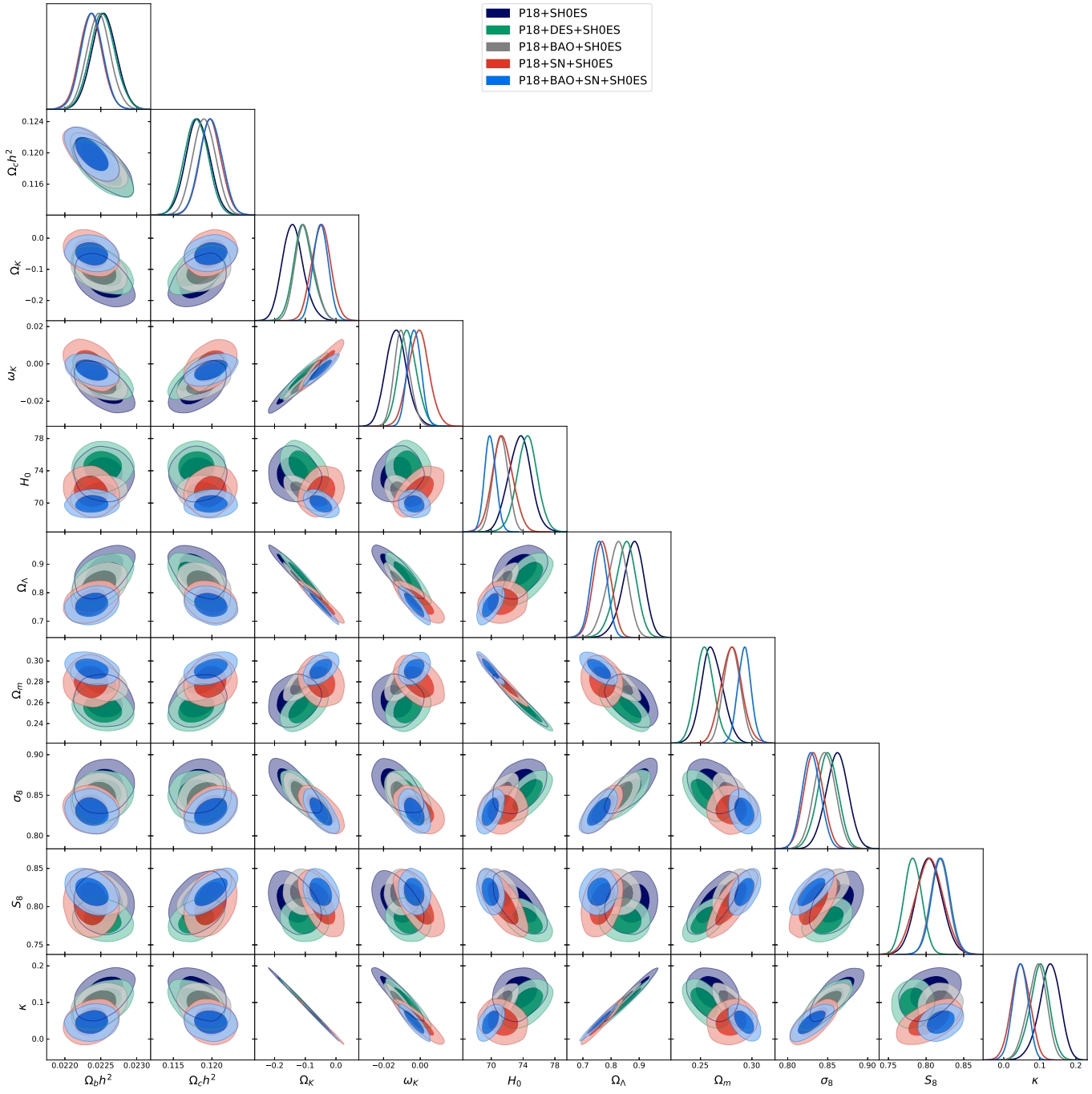


**Figure 1.** *Cont.*

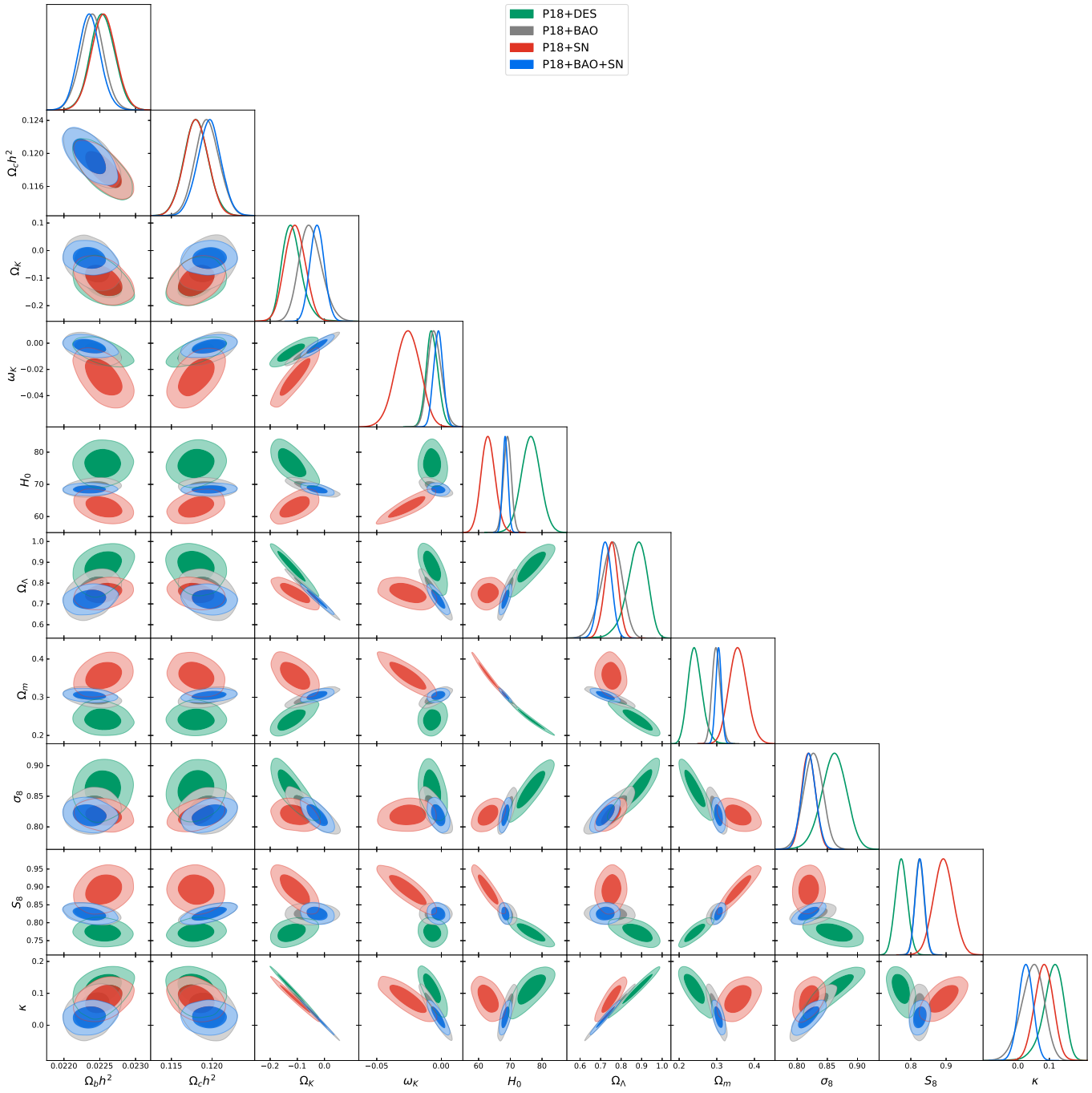


**Figure 1.** Confidence contours and posterior parameter distributions in Model 3: $\Omega_k \neq 0$ and $\omega_k \neq 0$.

## 4. Discussion

The standard GR-based *flat* ΛCDM model has been remarkably successful in describing a broad spectrum of cosmological phenomena probed with a wide variety of CMB projects, optical and IR telescopes, and extensive galaxy surveys, aiming for spectral and spatial mapping of the CMB and tracing the large-scale structure and evolution of the Universe. The KΛCDM model was a better fit for all dataset combinations than ΛCDM when the SH0ES prior was assumed, whereas the two models performed equally well when the SH0ES prior was not adopted. However, when the models were contrasted only with the P18 dataset without the SH0ES prior, there was a strong preference for KΛCDM. When the SH0ES prior was not included, the dataset combinations P18+BAO, P18+SN, and P18+SN+BAO showed no preference for KΛCDM over the simpler flat ΛCDM model.

Consequently, if the SH0ES prior was ignored in the analysis, then the concordance model converged on flat ΛCDM by default.

The unique spacetime metric that describes a maximally symmetric spatial hypersurface is the FRW metric, possibly having a non-vanishing (constant) spatial curvature. The curvature parameter appeared in both the Friedmann equation and geodesic equations, a single parameter that appeared in both the $t(z)$ and $r(t)$ relations and thus also in the $r(z)$ relation. In this work, we explored the consequences of adding an additional degree of freedom by allowing two independent curvature parameters in the $t(z)$ and $r(t)$ relations, as described in Section 3. We defined a derived 'anomaly' (the 'curvature slip') parameter $\kappa \equiv \omega_k - \Omega_k$ that quantified the degree of mismatch between these two parameters, which we inferred by determining the statistical significance of its departure from its canonical value of zero. The reference model, `Model 1`, was ΛCDM, and `Model 2` was KΛCDM. Our modified models were `Model 3`, in which both $\Omega_k$ and $\omega_k$ are free parameters. In `Model 4`, only $\Omega_k$ is a free parameter, whereas in `Model 5`, only $\omega_k$ is allowed to vary.

When the SH0ES prior was imposed, KΛCDM was clearly a better fit to the data than ΛCDM, as is evident from Table 3. `Model 3` performed much better with a DIC gain of $\gtrsim 20$ when neither BAO nor SN data were included. When these datasets were included, the gain reduced to ∼7–12, which was still better than KΛCDM. Remarkably, with just the P18+SH0ES data, `Model 3` resulted in $\kappa \neq 0$ having extremely high statistical significance, with betting odds worse than $1:10^7$ against $\kappa \neq 0$ (Table 4). A similar conclusion applies to P18+DES+SH0ES and P18+BAO+SH0ES but with lower statistical significance. `Model 4` and `Model 5` were also found to be statistically acceptable, though at a lower level of significance, as is apparent from the results listed in Tables 4 and 5.

For dataset combinations with no SH0ES prior, we found that none of `Models 3–5` provided a better fit for the data than `Model 2`. With these dataset combinations, `Model 3` did not provide a better fit over either `Model 4` or `Model 5`, except for the cases of P18+DES and P18+SN, for which there was strong evidence (supported by a DIC gain $\gtrsim 7$) in favor of this model over both KΛCDM and ΛCDM. We conclude that a model that allows for simultaneous variation of both $\Omega_k$ and $\omega_k$ is, in general, not warranted by data combinations that include BAO.

Even though the above analysis was based on the addition of a phenomenologically motivated parameter, it is nonetheless of interest to consider its possibly physical interpretations. As discussed above, the proposed models were better fits for the current datasets than KΛCDM and particularly ΛCDM when the SH0ES prior was imposed. Since $H_0$ and $\Omega_k$ were correlated in KΛCDM, imposing the SH0ES prior drove $\Omega_k$ to positive values (i.e., toward a preference for a hyperbolic topology). The $H_0 - \Omega_k$ correlation was intuitively clear; in a spatially closed Universe (i.e., $\Omega_k < 0$), incoming light rays are bent inward, the crossover time of a photon is longer, and consequently, $H_0$ is smaller. Therefore, a higher value of $H_0$ resulted in a higher value for $\Omega_k$. A sufficiently high value of $H_0$ necessarily led to $\Omega_k > 0$ (i.e., an open universe). Now, when both $\omega_k$ and $\Omega_k$ are allowed to simultaneously vary, even a flat geometry $\omega_k \approx 0$ (which favors a higher $H_0$ than in closed space due to the above-mentioned correlation) is possible, but it would still have an extremely negative $\Omega_k$ value that allows for a longer fly time for incoming photons. (In the extreme case where $\Omega_k$ is sufficiently negative (i.e., the Universe is strongly closed), the fly time could be infinite.) In the process, we can allow for a large $H_0$ value to still be consistent with an extremely negative $\Omega_k$ value without affecting the angular diameter distance and without having to compensate (by lowering the value of $H_0$) for the closed geometry simply because even though $\Omega_k$ can be significantly negative, $\omega_k$ can still satisfy $|\omega_k| \ll 1$.

Whereas the curvature slip considered in the present work was examined within the ΛCDM framework, the concept is clearly applicable to broader classes of cosmological

models. For instance, the Dark Energy Spectroscopic Instrument (DESI) collaboration has recently reported strong evidence for evolving dark energy within a spatially flat universe. Specifically, the equation of state (EOS) of the DE component $w(a) = w_0 + w_a(1 - a)$, where $w_0$ and $w_a$ are free model parameters, evolves with the scale factor in such a way that it behaves as a 'phantom' DE in the past [84]. Notably, this behavior has not been hitherto observed in other datasets. While the DESI collaboration has already considered models with nonzero spatial curvature, incorporating curvature slip could potentially further extend the space of viable models. Given that nonzero curvature slip is independently favored by several datasets, as illustrated in the present work, it would be natural to introduce this additional degree of freedom when analyzing the DESI data as well, potentially even providing an alternative explanation for what the DESI currently interprets as evidence for exotic dark energy evolution.

## 5. Summary

With the ever-increasing precision of cosmological observations, the challenge for ΛCDM is correspondingly higher. As the number and statistical significance of SM anomalies increase, so does the interest in alternative models. The SM is based on our best-tested theory of gravitation, GR, which withstood the test of time. However, GR is well tested only within our solar system, whereas on galactic and supergalactic scales, it has faired poorly, as manifested by the need to invoke the existence of CDM and DE. Whereas on the largest cosmological scales, these two mass-energy forms were described by only two new parameters and therefore added only slight complexity to the model, this is far from being the case on galactic scales, where CDM profiles have to be fit separately for each and every galaxy or cluster of galaxies. As argued here—and, to the best of our knowledge, nowhere else in the context of the present work—what is known as 'dark energy' (assuming its simplest form: a cosmological constant) could by itself represent a gravitational anomaly on the largest cosmological scales, rather than a genuine form of energy.

The P18 data strongly favor a spatially closed space but only with a relatively low value of $H_0$, which is at odds with local measurements of $H_0$. Other datasets (e.g., P18+DES) even favored an open Universe; only P18+SN supported the closed Universe model but at an extremely weak $\sim 1\sigma$ confidence level. The BAO dataset has played a (somewhat surprisingly) significant role in the acceptance of flat ΛCDM as the SM. It would be remarkable if indeed the Universe, with its (post-inflation) continuous growth of structure, has no appreciable departure from global spatial flatness. Yet, this is what the current varied datasets, interpreted within the framework of the GR-based SM, seem to suggest. In the present work, we relaxed the 'stiffness' of KΛCDM to test for the possibility that a less 'rigid' model better fit the data. In the process, we found that especially when local measurements of $H_0$ were adopted as a prior (in the statistical analysis), this generalized model better fit the data than KΛCDM and notably better than ΛCDM. This new anomaly, the 'curvature slip' (gauged by the departure of a newly introduced $\kappa$ parameter from its vanishing canonical value), is yet another in a growing list of SM anomalies that enhance the need for either new physics or more nuanced analyses within the realm of standard physics.

**Author Contributions:** Conceptualization, M.S. and Y.R.; methodology, M.S. and Y.R.; software, M.S.; validation, M.S. and Y.R.; formal analysis, M.S.; investigation, M.S. and Y.R.; resources, Y.R.; data curation, M.S.; writing—original draft preparation, M.S. and Y.R.; writing—review and editing, Y.R.; visualization, M.S. and Y.R.; supervision, Y.R.; project administration, Y.R.; funding acquisition, Y.R. All authors have read and agreed to the published version of the manuscript.

**Funding:** This research was supported by a grant from the Joan and Irwin Jacobs donor-advised fund at the JCF (San Diego, CA).

**Data Availability Statement:** The original contributions presented in the study are included in the article. Further inquiries can be directed to the authors.

**Acknowledgments:** Anonymous referees are gratefully acknowledged for their constructive reviews.

**Conflicts of Interest:** The authors declare no conflict of interest. The funders had no role in the design of the study; in the collection, analyses, or interpretation of data; in the writing of the manuscript; or in the decision to publish the results.

## References

1. Handley, W. Curvature tension: Evidence for a closed universe. *Phys. Rev. D* **2021**, *103*, L041301. [CrossRef]
2. Abdalla, E.; Abellán, G.F.; Aboubrahim, A.; Agnello, A.; Akarsu, Ö.; Akrami, Y.; Alestas, G.; Aloni, D.; Amendola, L.; Anchordoqui, L.A.; et al. Cosmology intertwined: A review of the particle physics, astrophysics, and cosmology associated with the cosmological tensions and anomalies. *J. High Energy Astrophys.* **2022**, *34*, 49. [CrossRef]
3. Di Valentino, E.; Anchordoqui, L.A.; Akarsu, Ö.; Ali-Haimoud, Y.; Amendola, L.; Arendse, N.; Asgari, M.; Ballardini, M.; Basilakos, S.; Battistelli, E.; et al. Cosmology Intertwined IV: The age of the universe and its curvature. *Astropart. Phys.* **2021**, *131*, 102607. [CrossRef]
4. Di Valentino, E.; Melchiorri, A.; Silk, J. Planck evidence for a closed Universe and a possible crisis for cosmology. *Nat. Astron.* **2020**, *4*, 196. [CrossRef]
5. Efstathiou, G.; Gratton, S. The evidence for a spatially flat Universe. *Mon. Not. R. Astron. Soc.* **2020**, *496*, L91. [CrossRef]
6. Dicke, R.H. *Memoirs of the American Philosophical Society, Jayne Lectures for 1969*; American Philosophical Society: Philadelphia, PA, USA, 1970.
7. Carroll, S.M. In What Sense Is the Early Universe Fine-Tuned? *arXiv* **2014**, arXiv:1406.3057. [CrossRef]
8. Evrard, G.; Coles, P. Getting the measure of the flatness problem. *Class. Quantum Gravity* **1995**, *12*, L93. [CrossRef]
9. Lake, K. The Flatness Problem and Λ. *Phys. Rev. Lett.* **2005**, *94*, 201102. [CrossRef]
10. Helbig, P. Arguments against the flatness problem in classical cosmology: A review. *Eur. Phys. J. H* **2021**, *46*, 10. [CrossRef]
11. Helbig, P. The flatness problem and the age of the Universe. *Mon. Not. R. Astron. Soc.* **2020**, *495*, 3571. [CrossRef]
12. Adler, R.J.; Overduin, J.M. The nearly flat universe. *Gen. Rel. Grav.* **2005**, *37*, 1491. [CrossRef]
13. Vagnozzi, S.; Loeb, A.; Moresco, M. Eppur è piatto? The Cosmic Chronometers Take on Spatial Curvature and Cosmic Concordance. *Astrophys. J.* **2021**, *908*, 84. [CrossRef]
14. Vagnozzi, S.; Di Valentino, E.; Gariazzo, S.; Melchiorri, A.; Mena, O.; Silk, J. The galaxy power spectrum take on spatial curvature and cosmic concordance. *Phys. Dark Universe* **2021**, *33*, 100851. [CrossRef]
15. Dhawan, S.; Alsing, J.; Vagnozzi, S. Non-parametric spatial curvature inference using late-Universe cosmological probes. *Mon. Not. R. Astron. Soc.* **2021**, *506*, L1. [CrossRef]
16. Cao, S.; Ryan, J.; Ratra, B. Using Pantheon and DES supernova, baryon acoustic oscillation, and Hubble parameter data to constrain the Hubble constant, dark energy dynamics, and spatial curvature. *Mon. Not. R. Astron. Soc.* **2021**, *504*, 300. [CrossRef]
17. Chudaykin, A.; Dolgikh, K.; Ivanov, M.M. Constraints on the curvature of the Universe and dynamical dark energy from the full-shape and BAO data. *Phys. Rev. D* **2021**, *103*, 023507. [CrossRef]
18. Bargiacchi, G.; Benetti, M.; Capozziello, S.; Lusso, E.; Risaliti, G.; Signorini, M. Quasar cosmology: Dark energy evolution and spatial curvature. *Mon. Not. R. Astron. Soc.* **2022**, *515*, 1795. [CrossRef]
19. Glanville, A.; Howlett, C.; Davis, T. Full-shape galaxy power spectra and the curvature tension. *Mon. Not. R. Astron. Soc.* **2022**, *517*, 3087. [CrossRef]
20. Liu, Y.; Cao, S.; Liu, T.; Li, X.; Geng, S.; Lian, Y.; Guo, W. Model-independent Constraints on Cosmic Curvature: Implication from Updated Hubble Diagram of High-redshift Standard Candles. *Astrophys. J.* **2020**, *901*, 129. [CrossRef]
21. Arjona, R.; Nesseris, S. Novel null tests for the spatial curvature and homogeneity of the Universe and their machine learning reconstructions. *Phys. Rev. D* **2021**, *103*, 103539. [CrossRef]
22. Gonzalez, J.E.; Benetti, M.; von Marttens, R.; Alcaniz, J. Testing the consistency between cosmological data: The impact of spatial curvature and the dark energy EoS. *J. Cosmol. Astropart. Phys.* **2021**, *2021*, 060. [CrossRef]
23. Acquaviva, G.; Akarsu, Ö.; Katırcı, N.; Vazquez, J.A. Simple-graduated dark energy and spatial curvature. *Phys. Rev. D* **2021**, *104*, 023505. [CrossRef]
24. Jesus, J.F.; Valentim, R.; Moraes, P.H.R.S.; Malheiro, M. Kinematic constraints on spatial curvature from supernovae Ia and cosmic chronometers. *Mon. Not. R. Astron. Soc.* **2021**, *500*, 2227. [CrossRef]
25. Yang, W.; Giarè, W.; Pan, S.; Di Valentino, E.; Melchiorri, A.; Silk, J. Revealing the effects of curvature on the cosmological models. *Phys. Rev. D* **2023**, *107*, 063509. [CrossRef]
26. Gao, C.; Chen, Y.; Zheng, J. Investigating the relationship between cosmic curvature and dark energy models with the latest supernova sample. *Res. Astron. Astrophys.* **2020**, *20*, 151. [CrossRef]

27. Zhang, Y.; Cao, S.; Liu, X.; Liu, T.; Liu, Y.; Zheng, C. Multiple measurements of gravitational waves acting as standard probes: Model-independent constraints on the cosmic curvature with DECIGO. *Astrophys. J.* **2022**, *931*, 119. [CrossRef]
28. Favale, A.; Gómez-Valent, A.; Migliaccio, M. Cosmic chronometers to calibrate the ladders and measure the curvature of the Universe. A model-independent study. *Mon. Not. R. Astron. Soc.* **2023**, *523*, 3406. [CrossRef]
29. Wang, Y.-J.; Qi, J.-Z.; Wang, B.; Zhang, J.-F.; Cui, J.-L.; Zhang, X. Cosmological model-independent measurement of cosmic curvature using distance sum rule with the help of gravitational waves. *Mon. Not. R. Astron. Soc.* **2022**, *516*, 5187. [CrossRef]
30. Liu, T.; Cao, S.; Biesiada, M.; Geng, S. Revisiting the Hubble Constant, Spatial Curvature, and Cosmography with Strongly Lensed Quasar and Hubble Parameter Observations. *Astrophys. J.* **2022**, *939*, 37. [CrossRef]
31. Di Valentino, E.; Melchiorri, A.; Silk, J. Investigating Cosmic Discordance. *Astrophys. J. Lett.* **2021**, *908*, L9. [CrossRef]
32. Tröster, T.; Asgari, M.; Blake, C.; Cataneo, M.; Heymans, C.; Hildebrandt, H.; Joachimi, B.; Lin, C.-A.; Sánchez, A.G.; Wright, A.H.; et al. KiDS-1000 Cosmology: Constraints beyond flat ΛCDM. *Astron. Astrphys.* **2021**, *649*, A88. [CrossRef]
33. Stevens, J.; Khoraminezhad, H.; Saito, S. Constraining the spatial curvature with cosmic expansion history in a cosmological model with a non-standard sound horizon. *J. Cosmol. Astropart. Phys.* **2023**, *2023*, 046. [CrossRef]
34. Guth, A.H. Inflationary universe: A possible solution to the horizon and flatness problems. *Phys. Rev. D* **1981**, *23*, 347. [CrossRef]
35. Gott, J.R. Creation of open universes from de Sitter space. *Nature* **1982**, *295*, 304. [CrossRef]
36. Bucher, M.; Goldhaber, A.S.; Turok, N. Open universe from inflation. *Phys. Rev. D* **1995**, *52*, 3314. [CrossRef]
37. Yamamoto, K.; Sasaki, M.; Tanaka, T. Large-Angle Cosmic Microwave Background Anisotropy in an Open Universe in the One-Bubble Inflationary Scenario. *Astrophys. J.* **1995**, *455*, 412. [CrossRef]
38. Yamauchi, D.; Linde, A.; Naruko, A.; Sasaki, M.; Tanaka, T. Open inflation in the landscape. *Phys. Rev. D* **2011**, *84*, 043513. [CrossRef]
39. Ratra, B. Inflation in a closed universe. *Phys. Rev. D* **2017**, *96*, 103534. [CrossRef]
40. Velten, H.; Caramês, T.R.P. To Conserve, or Not to Conserve: A Review of Nonconservative Theories of Gravity. *Universe* **2021**, *7*, 38. [CrossRef]
41. Rastall, P. Generalization of the Einstein Theory. *Phys. Rev. D* **1972**, *6*, 3357. [CrossRef]
42. Fabris, J.C.; Alvarenga, M.H.; Hamani-Daouda, M.; Velten, H. Nonconservative unimodular gravity: A viable cosmological scenario? *Eur. Phy. J. C* **2022**, *82*, 522. [CrossRef]
43. Bonder, Y.; Herrera, J.E.; Rubiol, A.M. Energy nonconservation and relativistic trajectories: Unimodular gravity and beyond. *Phys. Rev. D* **2023**, *107*, 084032. [CrossRef]
44. Fazlollahi, H.R. Non-conserved modified gravity theory. *Eur. Phys. J. C* **2023**, *83*, 923. [CrossRef]
45. Paiva, J.A.P.; Lazo, M.J.; Zanchin, V.T. Generalized nonconservative gravitational field equations from Herglotz action principle. *Phys. Rev. D* **2022**, *105*, 124023. [CrossRef]
46. Al-Rawaf, A.S.; Taha, M.O. Cosmology of General Relativity without Energy-Momentum Conservation. *Gen. Rel. Grav.* **1996**, *28*, 935. [CrossRef]
47. Smalley, L.L. Gravitational theories with nonzero divergence of the energy-momentum tensor. *Phys. Rev. D* **1975**, *12*, 376. [CrossRef]
48. Jones, J.; Copi, C.J.; Starkman, G.D.; Akrami, Y. The Universe is not statistically isotropic. *arXiv* **2023**, arXiv:2310.12859.
49. Sandage, A. The Change of Redshift and Apparent Luminosity of Galaxies due to the Deceleration of Selected Expanding Universes. *Astrophys. J.* **1962**, *136*, 319. [CrossRef]
50. Loeb, A. Direct Measurement of Cosmological Parameters from the Cosmic Deceleration of Extragalactic Objects. *Astrophys. J. Lett.* **1998**, *499*, L111. [CrossRef]
51. Liske, J.; Grazian, A.; Vanzella, E.; Dessauges, M.; Viel, M.; Pasquini, L.; Haehnelt, M.; Cristiani, S.; Pepe, F.; Avila, G.; et al. Cosmic dynamics in the era of Extremely Large Telescopes. *Mon. Not. R. Astron. Soc.* **2008**, *386*, 1192. [CrossRef]
52. Calabrese, E.; Slosar, A.; Melchiorri, A.; Smoot, G.F.; Zahn, O. Cosmic microwave weak lensing data as a test for the dark universe. *Phys. Rev. D* **2008**, *77*, 123531. [CrossRef]
53. Kable, J.A.; Addison, G.E.; Bennett, C.L. Deconstructing the Planck TT Power Spectrum to Constrain Deviations from ΛCDM. *Astrophys. J.* **2020**, *905*, 164. [CrossRef]
54. Vagnozzi, S. Bounds on light sterile neutrino mass and mixing from cosmology and laboratory searches. *Phys. Rev. D* **2021**, *104*, 063524. [CrossRef]
55. Ivanov, M.M.; Ali-Haïmoud, Y.; Lesgourgues, J. $H_0$ tension or $T_0$ tension? *Phys. Rev. D* **2020**, *102*, 063515. [CrossRef]
56. Bose, B.; Lombriser, L. Easing cosmic tensions with an open and hotter universe. *Phys. Rev. D* **2021**, *103*, L081304. [CrossRef]
57. Shimon, M.; Rephaeli, Y. Parameter interplay of CMB temperature, space curvature, and expansion rate. *Phys. Rev. D* **2020**, *102*, 083532. [CrossRef]
58. Kolb, E.W. A Coasting Cosmology. *Astrophys. J.* **1989**, *344*, 543. [CrossRef]
59. Buchert, T. Toward physical cosmology: Focus on inhomogeneous geometry and its non-perturbative effects. *Class. Quantum Gravity* **2011**, *28*, 164007. [CrossRef]
60. Clifton, T.; Ferreira, P.G. Archipelagian cosmology: Dynamics and observables in a universe with discretized matter content. *Phys. Rev. D* **2009**, *80*, 103503. [CrossRef]

61. Räsänen, S. Light propagation and the average expansion rate in near-FRW universes. *Phys. Rev. D* **2012**, *85*, 083528. [CrossRef]
62. Buchert, T.; Carfora, M.; Ellis, G.F.R.; Kolb, E.W.; MacCallum, M.A.H.; Ostrowski, J.J.; Räsänen, S.; Roukema, B.F.; Andersson, L.; A Coley, A.; et al. Is there proof that backreaction of inhomogeneities is irrelevant in cosmology? *Class. Quantum Gravity* **2015**, *32*, 215021. [CrossRef]
63. Agashe, A.; Ishak, M. An Almost FLRW Universe as an Averaged Geometry in Macroscopic Gravity. *Gravit. Cosmol.* **2023**, *29*, 110. [CrossRef]
64. Buchert, T. Dark Energy from structure: A status report. *Gen. Rel. Grav.* **2008**, *40*, 467. [CrossRef]
65. Buchert, T.; Larena, J.; Alimi, J.-M. Correspondence between kinematical backreaction and scalar field cosmologies—the 'morphon field'. *Class. Quantum Gravity* **2006**, *23*, 6379. [CrossRef]
66. Buchert, T. A cosmic equation of state for the inhomogeneous universe: Can a global far-from-equilibrium state explain dark energy? *Class. Quantum Gravity* **2005**, *22*, L113. [CrossRef]
67. Geshnizjani, G.; Chung, D.J.; Afshordi, N. Do large-scale inhomogeneities explain away dark energy? *Phys. Rev. D* **2005**, *72*, 023517. [CrossRef]
68. Kozaki, H.; Nakao, K.-I. Volume expansion of a Swiss-cheese universe. *Phys. Rev. D* **2002**, *66*, 104008. [CrossRef]
69. Nambu, Y. Back reaction and the effective Einstein equation for the universe with ideal fluid cosmological perturbations. *Phys. Rev. D* **2002**, *65*, 104013. [CrossRef]
70. Fleury, P. Cosmic backreaction and Gauss's law. *Phys. Rev. D* **2017**, *95*, 124009. [CrossRef]
71. Fleury, P.; Clarkson, C.; Maartens, R. How does the cosmic large-scale structure bias the Hubble diagram? *J. Cosmol. Astropart. Phys.* **2017**, *2017*, 062. [CrossRef]
72. Giblin, J.T.; Mertens, J.B.; Starkman, G.D. Departures from the Friedmann-Lemaitre-Robertston-Walker Cosmological Model in an Inhomogeneous Universe: A Numerical Examination. *Phys. Rev. Lett.* **2016**, *116*, 251301. [CrossRef] [PubMed]
73. Buchert, T. On Average Properties of Inhomogeneous Fluids in General Relativity: Dust Cosmologies. *Gen. Rel. Grav.* **2000**, *32*, 105. [CrossRef]
74. Ellis, G.F.R. Inhomogeneity effects in cosmology. *Class. Quantum Gravity* **2011**, *28*, 164001. [CrossRef]
75. Larena, J.; Alimi, J.-M.; Buchert, T.; Kunz, M.; Corasaniti, P.-S. Testing backreaction effects with observations. *Phys. Rev. D* **2009**, *79*, 8, 083011. [CrossRef]
76. Lapi, A.; Haridasu, B.S.; Boco, L.; Cueli, M.M.; Baccigalupi, C.; Danese, L. Little ado about everything. Part II. An 'emergent' dark energy from structure formation to rule cosmic tensions. *J. Cosmol. Astropart. Phys.* **2025**, *4*, 015. [CrossRef]
77. Aghanim, N.; Akrami, Y.; Arroja, F.; Ashdown, M.; Aumont, J.; Baccigalupi, C.; Ballardini, M.; Banday, A.J.; Barreiro, R.B.; Bartolo, N.; et al. [Planck Collaboration]. Planck 2018 results. I. Overview and the cosmological legacy of Planck. *Astron. Astrophys.* **2020**, *641*, A1. [CrossRef]
78. To, C.; Krause, E.; Rozo, E.; Wu, H.; Gruen, D.; Wechsler, R.H.; Eifler, T.F.; Rykoff, E.S.; Costanzi, M.; Becker, M.R.; et al. Dark Energy Survey Year 1 Results: Cosmological Constraints from Cluster Abundances, Weak Lensing, and Galaxy Correlations. *Phys. Rev. Lett.* **2021**, *126*, 141301. [CrossRef]
79. Alam, S.; Ata, M.; Bailey, S.; Beutler, F.; Bizyaev, D.; Blazek, J.A.; Bolton, A.S.; Brownstein, J.R.; Burden, A.; Chuang, C.-H.; et al. The clustering of galaxies in the completed SDSS-III Baryon Oscillation Spectroscopic Survey: Cosmological analysis of the DR12 galaxy sample. *Mon. Not. R. Astron. Soc.* **2017**, *470*, 2617. [CrossRef]
80. Ross, A.J.; Samushia, L.; Howlett, C.; Percival, W.J.; Burden, A.; Manera, M. The clustering of the SDSS DR7 main Galaxy sample—I. A 4 per cent distance measure at z = 0.15. *Mon. Not. R. Astron. Soc.* **2015**, *449*, 835. [CrossRef]
81. Beutler, F.; Blake, C.; Colless, M.; Jones, D.H.; Staveley-Smith, L.; Campbell, L.; Parker, Q.; Saunders, W.; Watson, F. The 6dF Galaxy Survey: Baryon acoustic oscillations and the local Hubble constant. *Mon. Not. R. Astron. Soc.* **2011**, *416*, 3017. [CrossRef]
82. Scolnic, D.M.; Jones, D.O.; Rest, A.; Pan, Y.C.; Chornock, R.; Foley, R.J.; Huber, M.E.; Kessler, R.; Narayan, G.; Riess, A.G.; et al. The Complete Light-curve Sample of Spectroscopically Confirmed SNe Ia from Pan-STARRS1 and Cosmological Constraints from the Combined Pantheon Sample. *Astrophys. J.* **2018**, *859*, 101. [CrossRef]
83. Liddle, A.R. Information criteria for astrophysical model selection. *Mon. Not. R. Astron. Soc.* **2007**, *377*, L74. [CrossRef]
84. Abdul-Karim, M.; Aguilar, J.; Ahlen, S.; Alam, S.; Allen, L.; Prieto, C.A.; Alves, O.; Anand, A.; Andrade, U.; Armengaud, E.; et al. [DESI Collaboration]. DESI DR2 Results II: Measurements of Baryon Acoustic Oscillations and Cosmological Constraints. *arXiv* **2025**, arXiv:2503.14738. [CrossRef]